PREPRINT UCRL- 79334

Lawrence Livermore Laboratory

ELECTROSTATIC ION CYCLOTRON WAVES AND
ION ENERGY DIFFUSION IN A MIRROR MACHINE

William C. Turner

August 1, 1977

JOURNAL d'PHYSIQUE - FRANCE

This paper was prepared for submission to IRAP Congress, June 27-July 3, 1977.
Third Congress, PMI Laboratory, Ecole Polytechnique, Palaiseau - France

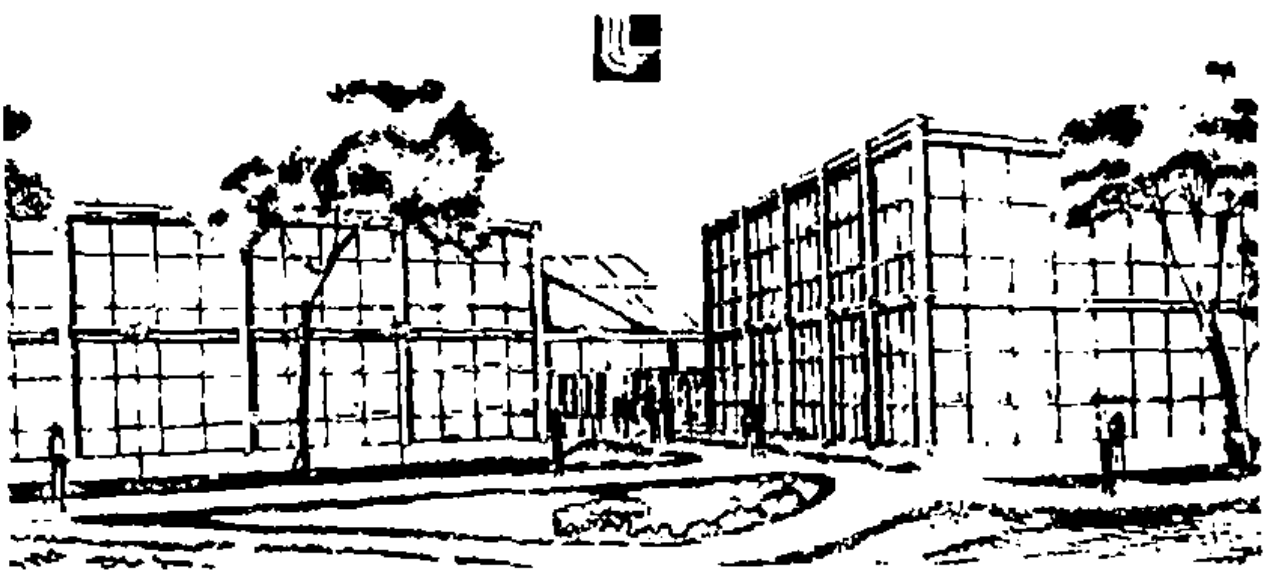

ELECTROSTATIC ION CYCLOTRON WAVES AND ION ENERGY DIFFUSION IN A MIRROR MACHINE

William C. Turner
Lawrence Livermore Laboratory

ABSTRACT

Measurements of ion cyclotron fluctuations and ion energy diffusion in the neutral beam injected 2XIIB mirror machine are presented. A narrow band single mode spectrum is always observed. When the plasma is de-stabilized by turning off axially injected streaming plasma, the wave amplitude increases and a simultaneous increase in ion-energy diffusion is observed. The spectral properties of the wave do not change. The data are in accord with a wave particle saturation of the drift cyclotron loss cone (DCLC) mode.

This work prepared for U.S. ERDA under contract No. W-7405-Eng-48

I. Introduction

In this paper we will discuss measurements of electrostatic ion cyclotron waves in a mirror machine and the observed increase of ion energy diffusion with increase in wave amplitude. The measurements were performed on the latest of a series of experiments at Livermore - the neutral beam injected 2XIIB experiment.[1] Similar observations have been reported in the PR-6 mirror experiment at Kurchatov.[2] The data support the theoretical interpretation of these experiments[3] which supposes a quasi-linear saturation of the drift cyclotron loss cone (DCLC) instability.[4] Following this section the main body of the paper is organized into four parts. Section II is an experimental overview of 2XIIB plasma conditions. Section III briefly describes the present theory of mirror machines. Sections IV and V present the detailed measurements of ion cyclotron waves and observation of ion energy diffusion respectively. The final section states the conclusions of this work.

II. Overview of 2XIIB Experiment

A schematic of the 2XIIB experiment is shown in Fig. 1. Deuterium plasma trapped in a minimum B magnetic well (center vacuum field 6.4 kg, mirror ratio R = 2.0, distance between mirrors L = 150 cm) is continuously driven by 12 LBL-type 50 amp 20 keV neutral beam injectors.[5] It is a pulsed experiment with vacuum field strength and neutral beam injected current held constant for 10 ms in the present mode of operation. In the earliest experiments on this device a target for neutral beam injection was formed by transit-time trapping and compression of plasma from fast-pulsed (10 μs) titanium-washer guns streaming along the 2 kg solenoidal guide field. In this mode of operation, without maintaining the flow of streaming plasma, neutral beam injection did not sustain the plasma and density decay times of a few hundred microseconds were observed. Subsequently it was discovered that if one of

the plasma guns was run in a long pulse mode, the amplitude of ion cyclotron oscillations was reduced and the plasma density would build up to a constant level for the duration of stream injection. When the stream plasma was shut off, the amplitude of ion cyclotron oscillations increased, and the plasma decayed as before. In this way, using up to three long-pulsed plasma guns, the plasma density was maintained for 5 ms at a peak density $n \sim 5 \times 10^{13}/cm^3$ and mean ion energy $\bar{E}_i \sim 13$ keV with approximately 250 amps equivalent D° injected neutral beam current. It was then found that the long pulse-stream plasma, injected after the pulsed mirror magnets reached full-field strength, was a suitable target for build-up by neutral beam trapping[6] and the transit-time target trapping with compression was discontinued. The peak density attained by plasma gun stream stabilization seemed, however, to be limited at high levels of neutral beam injection by periodic bursts ($\sim$100 μs) of ion cyclotron oscillations. To provide an increased warm plasma stream current a gas-feed system was installed near one of the mirror regions as shown in Fig. 1(b). Stream plasma is produced by electron ionization of the gas by plasma end-loss current. Using this gas feed system a peak plasma density $n \sim 1.5 \times 10^{14}/cm^3$ has been reached.[7] In this paper we will only present measurements with plasma gun stabilization since in that case it is possible to observe the plasma decay after abruptly shutting off the stream plasma.

Plasma measurements are shown in Fig. 2 as a function of time for one of a group of stream-stabilized shots during which machine parameters were held constant and most of the data reported in this paper were obtained. Stream and beam injection begin simultaneously and approximately 1.8 ms later the line density in Fig. 2(a) reaches its peak value 4.5×10^{14} cm^{-2} by build-up on trapped neutral beam current. The line density shown was measured by neutral beam attenuation along a radial chord through the plasma center. Similar measurements along adjacent chords spaced at 2 cm intervals indicate

a Gaussian (Fig. 7) radial density profile with mean radius $R_p = \frac{1}{n(o)} \int_{-\infty}^{+\infty} n(x)dx$ of 7 cm. Center plasma density n(o) can be obtained by dividing the line density in Fig. 2(a) by $\sqrt{\pi}\, R_p = 12.4$ cm. The plasma stream gun is shut off at 3.2 ms and shortly afterward the center plasma line density decays with 0.30 ms decay time, although neutral beam injection continues. There is ample evidence from measurements of plasma diamagnetism, absolute magnitude of fast-atom charge-exchange flux and absolute measurements of neutron production[8] that the plasma loss observed in Fig. 2(a) represents an increase in the hot plasma ion-loss rate and that the warm-stream plasma constitutes only a small fraction (~ 20%) of the peak density attained. The mean plasma ion energy, measured by a fifteen-channel fast-atom charge-exchange analyzer, and the magnitude of the 40 keV charge-exchange signal are shown in Fig. 2(b) and 2(c) respectively. At the peak-plasma density attained the mean plasma ion energy $\bar{E}_i$ = 13 keV, corresponding to a mean-ion gyroradius a_i = 3.6 cm in the vacuum magnetic field. The ratio of mean plasma radius to ion gyroradius is therefore $\frac{R_p}{a_i} = 2$, far below the lower limit[9] ($\frac{R_p}{a_i} \sim 60$) required for stability of the DCLC mode in the present density regime $\frac{\omega_{pi}^2}{\omega_{ci}^2} = 2 - 4 \times 10^4$. As the plasma density decays, the mean-ion energy is observed to increase and there is a large increase in the amplitude of the 40 keV charge-exchange flux signal, indicating an increase in ion-energy diffusion when the plasma stream is turned off. An accompanying increase of downward diffusion would lead to an increased loss current of particles reaching the loss-cone ambipolar hole from the hot plasma distribution. However, because of the low-energy particle sink at the ambipolar hole energy, downward diffusion does not increase the magnitude of charge-exchange flux in low energy channels. In Fig. 2(d) we have shown the amplitude of rf oscillations detected by a high-impedance electrostatic probe on the radial boundary of

the plasma at R_{probe} = 14 cm near the midplane between mirrors. As the plasma density builds up, the rf amplitude is high, and then decreases as the peak density is reached. The rf amplitude then shows a large increase during the plasma decay that is simultaneous with the observed heating of the ion distribution. The frequency of the rf oscillations lies in a narrow band near the fundamental of the ion cyclotron frequency, and except for measurements very early or late in time, the wave is observed to propagate in the direction of the ion diamagnetic drift current with a phase velocity close to that obtained by equating the ion diamagnetic drift frequency

$$\omega_i^* = k_\perp \frac{cE_i}{eB} \frac{1}{R_p}$$

to the ion cyclotron frequency.

Measurement of the axial length of the plasma provides an important clue regarding the ion velocity space transport processes which determine confinement. If the length is comparable to the distance between mirrors, then ion pitch angle scattering into the loss cone is important. If the length is short compared to the distance between mirrors, the ion angular distribution is confined to a narrow cone perpendicular to the magnetic field. Then the dominant confinement processes are those that govern energy transport since ions escape only when their energy falls below the positive ambipolar potential. For a mirror confined narrow angular distribution ion-energy transport occurs by wave diffusion and by ions slowing down on the less energetic electrons.

The axial length of the plasma has been measured by a movable microwave interferometer and by neutral-beam attenuation along axially displaced chords through the plasma. The characteristic length for the density to decrease by $\frac{1}{e}$ from the center is L_p = 12 - 16 cm and does not increase significantly

during the plasma decay. This length is short compared to the distance between mirrors (150 cm) but comparable to the $\frac{1}{e}$ half-width of the injected neutral current profile. Pitch angle scattering of energetic ions into the loss cone is therefore not a significant loss process, but rather ions are lost at low energy by wave diffusion or electron drag into the ambipolar hole. This conclusion is supported by direct measurement of the loss current energy spectrum with a gridded electrostatic analyzer outside the mirrors. A broad spectrum from 100 eV to 700 eV was measured.[10]

Electron temperature, measured by Thomson scattering, falls in the range 50 eV < KT_e < 90 eV during the time the plasma stream gun is on.[11] Detailed measurements of electron temperature after the stream is turned off have not been made; however, measurements without stream stabilization showed T_e rising from 60 eV to 140 eV during the density decay. The slowing down time of ions on the cooler electrons has been measured[12] for 20 < KT_e < 100 eV and found to follow the classical Spitzer $(KT_e)^{3/2}$ dependence.[13] The measured slowing-down times are also in numerical agreement with the Spitzer equation $n\tau_{ie} = 4.4 \times 10^7 (KT_e)^{3/2}$, KT_e in electron volts, when orbit average effects are included.

III. Theoretical Summary

We will now discuss the theory of mirror machines that is important for understanding our measurements. First a summary of the quasi-linear theory is given[3] and then we estimate the time scales of the ion transport processes and the frequencies relevant to the ion motion in 2XIIB.

The most important element of the recent quasi-linear theory of mirror machines[3] compared to earlier treatment of the DCLC instability[14,15] was the realization that the unstable plasma could maintain a narrow ion-angular distribution, since for $KT_e \ll \bar{E}_i$ the dominant transport processes are electron drag which change the particle speed, and wave diffusion, which acts

primarily on the velocity component perpendicular to B. According to the theory of a decaying plasma without neutral beam and plasma stream injection, wave diffusion grows to the level required to partially fill only the ambipolar hole region of velocity space $v_\perp^2 < \frac{1}{R-1}\frac{2e\phi}{M_i}$, rather than the entire loss cone, and the rate of diffusion need only match the transit time loss rate of particles with roughly the ambipolar energy, rather than the mean-ion energy. In this way plasma lifetimes of a few hundred microseconds were calculated, in agreement with the 2XII experimental data.[16] The earlier theory theory[14,15] of the DCLC instability supposed that the entire loss-cone had to be filled and predicted lifetimes of only a few axial bounces. For the case of neutral beam injection, as in 2XIIB, a narrow ion angular distribution is created by neutral beam injection. However, without an external stream, the loss current of particles required to fill the ambipolar hole exceeds the trapped beam current required by diffusion from the hot-ion distribution. With the improved hot-ion confinement, steady-state densities are possible.

We briefly summarize the equations given in Ref. 3. For a $k_\parallel = 0$ mode, the DCLC dispersion relation in the local approximation is

$$1 + \frac{\omega_{pe}^2}{\omega_{ce}^2} + \frac{\omega_{pi}^4}{\omega_{ci}^2 k_\perp^2 c^2} - \left(1 + \frac{\omega}{2}\right)\frac{\omega_{pi}^2}{\omega_{ci} k_\perp R_p} + \frac{M_i \omega_{pi}^2}{k_\perp^2} F(0) \qquad (1)$$

$$+ \frac{\omega_{pi}^2}{k_\perp^2} \sum_{n=-\infty}^{+\infty} \int_0^\infty dE_\perp \frac{J_n^2\left(\frac{k_\perp}{\omega_{ci}}\sqrt{\frac{2E_\perp}{M_i}}\right)}{\omega - n\omega_{ci} + i\nu_{n,k}} \left[M_i \frac{\partial F}{\partial E_\perp} + \frac{k_\perp (1 - \frac{\omega_0}{2})f}{\omega_{ci} R_p}\right] = 0$$

Here, $F(E_\perp) = \int \frac{dE}{\sqrt{E_\parallel}}\, F(E_\perp, E_\parallel)$, $\int = \int F(E_\perp)\, dE_\perp$, R_p = radial scale length.

$E_\perp = B\left(n - \frac{\langle E_\perp \rangle}{\theta^2}\right)$ and $\Delta_{n,k}$ is a correlation width.

Assuming that $Re\,\omega = N\omega_{ci}$, $Im\,\omega = \gamma \ll Re\,\omega$ we obtain from Eq. (1),

$$\left\{ \frac{\omega_{pi}^4}{\omega_{ci}^2 c^2} + N_i^2 \omega_{pi}^2 F(0) + \omega_{pi}^2 \sum_{n \neq N} \int_0^\infty dE_\perp \frac{J_{n-N}^2}{(n-N)} \left[N_i N \frac{\partial F}{\partial E_\perp} - \frac{k_\perp (1 - \frac{\eta_g}{2}) F}{\omega_{ci} R_p} \right] \right\} \frac{1}{k_\perp^2}$$

$$- \left(1 + \frac{\epsilon_\perp}{2}\right) \frac{\omega_{pi}^2}{N\omega_{ci}^2 R_p} \frac{1}{k_\perp} + 1 + \frac{\omega_{pe}^2}{\omega_{ce}^2} = 0 \qquad (2)$$

$$\frac{\gamma_{n,k_\perp}}{N\omega_{ci}} = \frac{\pi \omega_{ci} \Gamma_p}{\left(1 + \frac{\epsilon_\perp}{2}\right)} \frac{1}{k_\perp} \int_0^\infty dE_\perp \frac{J_{N-n}^2}{\left(\frac{\omega_{n,k_\perp}}{N\omega_{ci}}\right)} \left\{ N_i N \omega_{ci} \frac{\partial F}{\partial E_\perp} + \frac{k_\perp (1 - \frac{\eta_g}{2}) F}{\omega_{ci} R_p} \right\} \qquad (3)$$

Eq. (2) is a transcendental equation that can be solved numerically for $k_\perp$ for an assumed ion energy distribution $F(E_\perp)$. This will be done below. Eq. (3) shows that the growth rate contains a loss cone term depending on $\frac{\partial F}{\partial E_\perp}$ and a drift term depending on the radial density gradient. The drift term (H. Berk private communication) contains a parameter $\eta_g = \frac{d}{dr}\left(\ln \frac{E_i}{n}\right)$. The quasi-linear transport equation describing evolution of the ion distribution

function is [17]

$$\frac{\partial F}{\partial t}(E_\perp,t) = \frac{\partial}{\partial E_\perp}\left(D\frac{\partial F}{\partial E_\perp} + \frac{k_\perp(1-\frac{\omega_g}{2})}{\omega_{ci}^2 R_p} DF\right) + \frac{\partial}{\partial E_\perp}\left(\frac{E_\perp F}{\tau_{ie}}\right) + n[S_i(E_\perp)$$

$$+ S_{cx}(E_\perp)] - F\int_0^\infty dE_\perp' S_{cx}(E_\perp') + J_{stream} - \nu_{transit} F$$

$$- \frac{F}{\tau_{cxg}} + g(E_\perp)\int_0^\infty dE_\perp \frac{\Gamma(E_\perp)}{\tau_{cxg}} \quad . \qquad (4)$$

The first term in Eq. (4) contains the quasi-linear diffusion coefficient, with the addition of a gradient dependent diffusion term (H. Berk, private communication), summed over wave numbers and ion cyclotron harmonics.

$$D(E_\perp) = \sum_{n,k_\perp} e^2 n^2 \omega_{ci}^2 \frac{|\phi_{n,k_\perp}|^2}{\omega_{n,k_\perp}} J_n^2\left(\frac{k_\perp}{\omega_{ci}}\sqrt{\frac{2E_\perp}{M_i}}\right) \quad . \qquad (5)$$

where $\phi_{n,k}$ is the potential fluctuation amplitude. The second term in Eq. (5) is the Spitzer electron drag term[13] where $\tau_{ie} = 4.4 \times 10^7 (KT_e)^{3/2}$ with KT_e in electron volts. The next three terms describe trapping of neutral beams by ionization and by charge-exchange replacing a distribution particle by a beam particle with source currents $nS_i(E_\perp)$ and $nS_{cx}(E_\perp)$ respectively. J_{stream} is the warm plasma stream source current and $J_{transit} = \nu_{transit} F(E_\perp)$ is the transit time loss current of ions below the ambipolar energy, with $\nu_{transit}$ equal to the inverse transit time. The last two terms allow for charge exchange with background gas.

From Ref. 3 an approximate estimate of the fraction of plasma required to fill the ambipolar hole is given as $\eta = \frac{1}{2(R-1)}\frac{e\phi}{E_i}$, where ϕ is the

the ambipolar potential and $\bar{E}_i$ the mean ion energy. If it is assumed that the warm plasma filling the ambipolar hole is Maxwellian with $KT = e\phi/(R-1)$, then a formula for the loss current required by marginal stability can be derived. The result is

$$I_{loss} = \frac{en}{\sqrt{2\pi M_i}} \cdot \frac{1}{\bar{E}_i}\left(\frac{e\phi}{R-1}\right)^{3/2} A_p \qquad (6)$$

where $A_p = \pi R_p^2$ is the plasma cross-sectional area. Using this formula we can estimate a particle loss time $\tau_{loss} = \frac{enV_p}{I_{loss}}$, where V_p = plasma volume. In mirror machines a positive ambipolar potential $e\phi \approx 4KT_e$ is required to balance the electron and ion loss rates. Inserting parameter values $R = 2$, KT_e = 75eV, $\bar{E}_i$ = 13 keV, $R_p = 7$ cm and $V_p = 4000$ cm^3 gives $\tau_{loss} \approx 0.23$ ms. This rough estimate is comparable to the loss rate observed in Fig. 2(a) when the external plasma stream is turned off.

In Table 1 we have summarized characteristic times for the physical processes in Eq. (4). Excluding the transit time of low-energy particles in the ambipolar hole, the fastest times are associated with beam injection. There are two beam injection times: the time for charge-exchange replacement of the plasma by beam atoms, and the time for build-up of plasma density by ionization trapping of beam atoms. Charge-exchange replacement of plasma ions by beam injected neutrals maintains a narrow ion-angular distribution and contributes energy to the plasma, since the mean beam atom energy is greater than the mean-ion energy. The parameter f appearing in the beam charge exchange and ionization times is the trapping efficiency, relative to a chord through the plasma center averaged over beam and plasma profiles. The beam-trapping formulas apply to the thin plasma limit and are approximately valid for central line density less than 5×10^{14} cm^{-2}. The mean time for charge-exchange erosion of the plasma by background gas is calculated from the cold-

TABLE 1. Plasma Time Scales *

Process			Time
Charge exchange replacement by a beam atom	$(\tau_{cx})_{\text{beam atom}} = \frac{eV_p}{f(2R_p\sigma_x)I_b}$	=	0.35 ms
Build-up rate by ionization of beam atoms	$\tau_{ib} = \frac{eV_p}{f(2R_p\sigma_i)I_b}$	=	1.0 ms
Electron drag	$\tau_{ie} = 2.3 \frac{4.4 \times 10^7 (KT_e)^{3/2}}{n(o)}$	=	3.5 ms
Charge exchange replacement by a cold gas atom	$(\tau_{cx})_{\text{gas atom}} = \frac{eR_p}{2j_g}$	=	3.6 ms
Transit time	$\tau_{\text{transit}} = \frac{L_p}{\sqrt{\frac{2eV_p}{M_i}}}$	=	0.002 ms
Ion-ion scattering time	$\tau_{ii} = 2.3 \frac{2 \times 10^{10} (E_i)^{3/2} \log_{10} R}{n(o)}$	=	23.0 ms

* The following parameters are assumed

$V_p = 4 \times 10^3$ cm^3	$\sigma_x = 1.2 \times 10^{-15}$ cm^2	f = 0.4
$R_p = 7$ cm	$\sigma_i = 4.0 \times 10^{-16}$ cm^2	$KT_e = 100$ eV
$L_p = 15$ cm	$I_b = 280$ amps	$E_i = 13$ keV
R = 2.0	$j_g = 5.0 \times 10^{-3}$ amps/cm^2	$n(o) = 3.5 \times 10^{13}$ cm^{-3}

TABLE 2. Typical Ion Frequencies in 2XIIB*

Frequency		Value
Ion cyclotron	$f_{ci} = \frac{1}{2\pi} \cdot \frac{eB_0}{M_i c}$	4.88 MHz
Ion plasma	$f_{pi} = \frac{1}{2\pi} \sqrt{\frac{4\pi ne^2}{M_i}}$	880 MHz
Ion bounce	$f_b = \frac{1}{2\pi L_B} \sqrt{\frac{2\bar{E}_\perp}{M_i}}$	240 kHz
∇B precession	$f_{\nabla B} = \frac{1}{2\pi} \frac{c\bar{E}_\perp}{eB_0} \frac{1}{R_B^2}$	21 kHz
ExB drift	$f_{ExB} = \frac{1}{2\pi} \frac{c\bar{E}_\perp}{eB_0} \frac{1}{R_p^2}$	25 kHz

* The following parameters are assumed:

$B_0 = 6.4$ kg

$n = 3.5 \times 10^{13}$ cm^{-3}

$\bar{E}_\perp = 13$ keV

$L_B = 75$ cm

$R_B = 55$ cm

$\bar{e}_\parallel = 500$ eV

gas flux ϕ_g measured by an absolutely calibrated fast-atom analyzer.[18] The transit time loss of a particle in the ambipolar hole gives a rough estimate of the diffusion times that will be required for the plasma to reach a marginally stable state. The factors $2\sqrt{2}$ in the collision times τ_{ie}, τ_{ii} arise from averaging over Gaussian density profiles, which increases the scattering times compared to those calculated for the center density n(o). Ion-ion Coulomb scattering is a negligible transport process compared to the other processes in Table 1.

In Table 2 we have estimated frequencies relevant to the ions in 2XIIB. For the ion bounce motion along field lines, the vacuum field axial magnetic well is represented by the parabolic form $B_o(1 + \frac{z^2}{L_B^2})$ with L_B = 75 cm. A radial well $B = B_o(1 + \frac{r^2}{R_B^2})$, R_B = 55 cm is used to compute the ∇B precession frequency. E x B drift in the positive ambipolar potential ϕ is estimated for a radial electric field $E_r = \frac{\phi}{R_p}$ with R_p = mean plasma radius. The ∇B and ExB drift motions have quite low frequencies, of the order 20 kHz. Doppler shift corrections to the ion cyclotron wave measurements due to ExB drift are expected to be negligible.

IV. Measurements of Wave Properties

To measure the frequency and wave length of the ion-cyclotron fluctuations we have used a technique similar to that used by Simonen[19] to measure azimuthal wavelength in the 2XII experiment. The 2XII measurements were obtained from oscilloscope waveforms detected by a double-tipped electrostatic probe outside the mirrors. The present measurements use a five-tip probe located on the radial boundary of the plasma between the mirrors. The data are recorded and analyzed using digital spectral analysis techniques.[20]

A diagram of the experimental method is given in Fig. 3. The five-channel probe is located radially at R_{probe} = 14 cm from the plasma axis and is displaced axially 4 cm from the vertical plasma midplane between the mirrors, on the side opposite stream gun injection. The probe tips are 1 cm long tungsten wires, 0.1 cm in diameter and adjacent tip separation is 1 cm. The tips have 10k input impedance, which is large compared to the expected plasma sheath resistance,[21] and flat frequency response up to 100 MHz. The probe measures azimuthal propagation across field lines. After amplification, the raw data are recorded on transient recorders (50 MHz digitizing rate, 2048-word memory) and processed by an on-line computer. The recorders therefore provide a 40.96 μs time window of the plasma oscillations on a particular shot. Data have been obtained over a sequence of shots, holding machine parameters constant, and varying the recorder trigger time. The trigger times for the data to be presented are shown as tick marks on the time base of Fig. 2(d). Instrumental time delay between recording channels will show up as phase shift not related to the plasma and can cause spurious effects. For example, a one-clock cycle (20ns) relative delay between recorders corresponds to a phase shift of $\pi/8$ = 0.63 radian at f = 5.0 MHz. We have therefore taken precautions to assure that the data can be referred to a common time base. The cable lengths from the probe to the amplifier inputs are matched. Equal time fiducial pulses are mixed with the data at the amplifier inputs to allow corrections for relative amplifier delay and time-base delay between recorder channels. Generally the time shift corrections applied to the data correspond to one-clock cycle phase shift or less. The probe signals are also passed through broad band frequency filters and detectors so that the envelope of oscillation can be recorded for the entire duration of a shot, as in Fig. 2(d).

Evidence that the oscillations detected by the probe are driven by the hot interior plasma and are not merely a local phenomenon at the probe position come from: (1) agreement with the frequency of oscillation detected by a similar probe located outside the mirrors but on field lines passing through the central hot plasma; (2) agreement, at lower densities than reported here, between phase modulation frequency of a 4 mm microwave interferometer and the frequency detected by probes;[22] and (3) the observed dependence of oscillation frequency on magnetic field depression by the central plasma beta (Fig.6).

The raw data are processed by computing the discrete Fourier transform $\phi_j(f_\alpha)$[23] from the time-domain data $\phi_j(t_\beta)$ for each probe channel j using a fast Fourier transform algorithm.

$$\phi_j(f_\alpha) = \frac{1}{N} \sum_{\beta=1}^{N} e^{-i2\pi\alpha\beta/N} \phi_j(t_\beta) \tag{7}$$

where $f_\alpha = \frac{\alpha}{N\Delta t}$, $1 \le \alpha \le \frac{N}{2}$ and $t_\beta = \beta\Delta t$ with sample interval $\Delta t = 20$ ns.

Cross-power spectra are then computed according to

$$P_{j1}(f_\alpha) = \phi_1^*(f_\alpha)\,\phi_j(f_\alpha) = |P_{j1}(f_\alpha)|\, e^{i\theta_{j1}(f_\alpha)}. \tag{8}$$

The amplitude spectrum $|P_{j1}(f_\alpha)|$ and phase spectra $\theta_{j1}(f_\alpha)$ $2 \le j \le 5$ are shown in Fig. 4 for a particular case. In a local plane wave representation, the phase spectrum is related to the local wave number $k(f_\alpha)$ by $\theta_{j1}(f_\alpha) = k(f_\alpha)\Delta x_{j1}$ where Δx_{j1} is the probe tip separation. The data in Fig. 4 have been calculated with N = 512 and averaging the cross-power spectrum over the four segments of transient recorder memory. No window correction has been applied to reduce leakage due to the finite length time sample.

The amplitude spectrum in Fig. 4(a) has a very narrow frequency component at f = 4.50 MHz, close to the deuteron vacuum field cyclotron frequency f = 4.88 MHz. The FWHM at 6 dB is approximately 100 kHz, about equal to the width due to the finite time sample. We therefore conclude that the true line width is characterized by $\frac{\Delta f}{f} < 0.02$. There is a second peak in the amplitude spectrum at twice the fundamental frequency f = 9.0 MHz that is reduced by 18 dB relative to the fundamental. Higher harmonics are suppressed even further. We have not been able to attribute significance to the near zero frequency peak which is sometimes present and sometimes not. We do not observe a spectral broadening as the amplitude of oscillation builds up during the decay. In general the harmonics are suporessed > 10 dB relative to the fundamental and the observed widths of the fundamental are accounted for by the finite time domain sample.

The phase spectra in Fig. 4(b), evaluated at the peak power frequency f = 4.50 MHz increase with probe-tip separation. The probe tips were oriented perpendicular to field lines and after correction for relative time-base delay, a least square fit gives $k_\perp = 0.51 \pm 0.10\ cm^{-1}$ at the 14 cm radial position of the probe. The sign of the phase shift gives the direction of propagation. For the conventions used, the positive phase shifts in Fig. 4(b) indicate the wave is propagating azimuthally in the direction of the ion-diamagnetic drift current.

The wave numbers are summarized for all of the data in Fig. 5. The measurements have been scaled with the ratio

$$\frac{R_{probe}}{R_{plasma}} = \frac{14\ cm}{7\ cm} = 2.0.$$

Positive wave numbers correspond to propagation in the ion-diamagnetic direction.

Except for measurements very early or late in time the direction of azimuthal propagation is in the direction of the ion diamagnetic current. This corresponds to the prediction of the DCLC dispersion relation given by Eq. (1). The explanation for propagation opposite the ion diamagnetic drift early and late in time is not known.

The observed frequencies of oscillation are always less than the vacuum field cyclotron frequency. Fig. 6 provides a simple explanation, attributing the frequency shift from the vacuum cyclotron frequency to depression of the vacuum field by finite plasma beta $\beta = 8\pi \frac{n\bar{E}_i}{B_{vac}^2}$. In Fig. 6 we have plotted the observed frequency shift vs. the product of mean-ion energy and line-density through the plasma center $\bar{E}_i \int n dl$. Beta at the plasma center is related to this variable by

$$\beta(0) = \frac{8\pi}{\sqrt{\pi}\, R_{plasma}} \frac{\bar{E}_i \int n dl}{B_{vac}^2}$$

and is indicated along the horizontal axis at the top of Fig. 6 for R_{plasma} = 7 cm and B_{vac} = 6.4 kg. We have also plotted in Fig. 6 two curves showing the expected frequency shift in the long thin plasma approximation $\frac{\Delta f}{f_o} = 1 - \sqrt{1-\beta}$. The solid curve is for the central plasma beta $\beta(0)$ while the dashed curve is for the density weighted average plasma beta $\beta = \frac{\beta(0)}{2}$. Since most of the observed frequency shifts lie close to the expectation for the central plasma beta, the data suggest that the oscillations are more

closely related to the center plasma density rather than the density further out on the plasma profile where the density gradient is steeper.

The perpendicular wave numbers for propagation in the ion diamagnetic drift direction in Fig. 5 fall close to the value obtained by equating the ion diamagnetic drift frequency

$$\omega_i^* = k_\perp \frac{cE_i}{eB} \cdot \frac{1}{R_{plasma}}$$

to the cyclotron frequency $\omega_{ci} = eB/M_i c$. For E_i = 13 keV, B = 6.4 kg, R_{plasma} = 7 cm, this condition yields $k_\perp = 1.06\ cm^{-1}$. The correlation of the oscillation frequency with the center plasma density seems unusual for a drift wave. This behavior may be due to the rather small ratio of plasma radius to mean-ion gyroradius $\frac{R_{plasma}}{a_i} = 2$ and the proposed quasilinear saturation of this mode[3] which requires a certain density ratio $\frac{e_i}{E_i}$ of warm plasma filling the ambipolar hole compared to the hot-plasma. If this condition is least well attained by external stream plasma injection at the center of the plasma, then the driving mechanism for the instability would be strongest at the plasma center. A related phenomenon is observed in Fig. 7 where we have plotted radial line density profiles at various times. Early in the decay the plasma density decrease is largest at the plasma center and then moves radially outward.

In Fig. 8(a) we have plotted normalized ion energy distributions before the decay and late in the decay. The azimuthal phase velocities of the waves propagating in the ion-diamagnetic drift direction in Fig. 5 match the ion speed in the range $0.35 \cdot E_i < 1.5$ keV. This range of speeds encompasses the cutoff that is generally observed in the charge-exchange flux spectrum near 500 eV.

To compare with the wave number measurements in Fig. 5 we have performed a marginal stability analysis of the DCLC dispersion relation given in Eq. 1. To perform the integrals over the ion distribution function, we have chosen the following functional form that models the observed charge-exchange spectrum and includes a warm component for stability.

$$F(E_\perp) = \frac{\alpha}{1+\alpha}\,\frac{1}{E_W}\,e^{-E_\perp/E_W} + \frac{1}{1+\alpha}\,\frac{1}{E_H^2}\,H(E_\perp - e\phi)\,E_\perp e^{-E_\perp/E_H} \tag{9}$$

$$H(E_\perp - e\phi) = \begin{cases} 1 & E_\perp \geq e\phi \\ 0 & E_\perp < e\phi \end{cases}$$

The coefficient α is fixed by normalization $\int_0^\infty F(E_\perp)\,dE_\perp = 1.0$. The mean energy of the hot component in Eq. (9) is $\langle E_\perp \rangle = 2E_H + \frac{(e\phi)^2}{E_H + e\phi}$. This distribution is plotted in Fig. 8(b) for $\langle E_\perp \rangle = 13$ keV, $e\phi = 0.5$ keV, $\alpha = 0$. For $Re\,\omega = \omega_{ci}$, Eq. (2) is solved for $k_\perp$ and Eq. (3) for the growth rate γ. The solution is iterated by increasing the warm plasma fraction α until $\gamma = 0$. The solution depends on the mean energy of the warm component E_W, the ambipolar potential ϕ and the mean energy of the hot component $\langle E_\perp \rangle$ as shown in Fig. 9. Positive $k_\perp$ corresponds to propagation in the ion diamagnetic drift direction. The solution is observed to depend rather weakly on E_W and $e\phi$. The magnitude of the computed $k_\perp$ and its $\sim \langle E_\perp \rangle^{-\frac{1}{2}}$ dependence fall within $\sim$ 30% of the previously mentioned condition of equating the ion diamagnetic drift frequency to the ion cyclotron frequency. Furthermore, for $\langle E_\perp \rangle = 13$ keV the magnitude of the solution $k_\perp \sim 0.7$ cm^{-1} is in the range of values observed in Fig. 5 for propagation in the ion-diamagnetic drift direction. The warm plasma fraction required for stability in these calculations falls in the range $0.03 < \alpha < 0.06$. The dispersion relation calculations in Fig.9 were done for $n = 3.6 \times 10^{13}$ cm^{-3}, $R_p = 7$ cm and $\phi_p = 0$. Reducing n a factor of 2 lowers $k_\perp$ by 7 percent. Setting $\phi_p = 0.5$ lowers $k_\perp$ by 10 percent.

A narrow ion cyclotron spectrum and azimuthal propagation in the ion diamagnetic drift direction, similar to some of the measurements reported here, have been observed near onset of a current-driven instability in a Q machine.[24] The mode was identified as an ion cyclotron drift wave (ICDW). In that case the driving mechanism that couples to the drift wave is an electron parallel current rather than the velocity space loss cone that is present here.

An ion cyclotron wave, with $k_\perp a_i \sim 4$, and propagating in the ion diamagnetic direction was also observed in the 2XII mirror experiment which did not employ intense neutral beam injection or stream stabilization. The plasma in 2XII decayed with a lifetime of a few hundred microseconds [16] after transit time trapping and compression. Simonen identified the wave as the DCLC mode.[19]

The width of the observed frequency spectrum, which is less than the ion bounce frequency computed for a mean-ion energy $\bar{E}_i = 13$ keV, raises some question about the applicability of stochastic diffusion modeled in the quasi-linear diffusion equation. Rosenbluth[25] has given a rough formula for a critical level of single mode coherent oscillation that is resonant with the ion cyclotron period at the midplane between mirrors.

$$\frac{e\phi_{crit}}{\bar{E}_i} = \left(\frac{a_i}{L_B}\right)^{5/3}$$

a_i is the ion gyroradius, L_B the magnetic field axial scale length, $B = B_o\left(1 + \frac{z^2}{L_B^2}\right)$. Below the critical level the particle motion is "superadiabatic"[26] and particles do not diffuse out of the system. Above the critical level stochastic diffusion applies. For 2XIIB, $a_i \sim 3.5$ cm, $L_B = 75$ cm, $\bar{E}_i = 13$ keV we obtain $\phi_{crit} \sim 80$ volts. Potential oscillations on the plasma boundary are generally less than ϕ_{crit} but it does not seem unreasonable that they exceed 80 V in the interior. Superadiabatic effects may therefor be present, but are probably not dominant. Further evidence of this is the

experimentally observed simultaneous increase of oscillation amplitude and ion energy diffusion, presented in the following section, during the plasma decay. The question of a possible difference in the form of diffusion coefficient that follows from Rosenbluth's analysis[25] compared to the quasi-linear diffusion coefficient in Eq. 5 has not been investigated in detail.

IV. Ion Energy Diffusion

According to quasi-linear theory,[3] a mirror plasma evolves to a marginally stable state by filling in the ambipolar hole of the ion-energy distribution. The warm plasma filling the ambipolar hole can be supplied either by diffusion from the hot-ion population at the expense of confinement or by an external plasma stream, in which case hot ion confinement is improved. Finite amplitude wave oscillations are generally expected to be present, either to diffuse hot ions into the ambipolar hole or to adjust the energy distribution of the stream injected ions to satisfy marginal stability. If the theory is correct, then wave-particle coupling should always result in some level of ion diffusion. The diffusion is most conveniently observed in the high-energy tail of the ion distribution where we do not have to contend with a particle sink that is present at low energy. The energy spectra in Fig. 8(a), where we note that 25 keV ions are present during and after stream injection although no ions are injected with energy greater than 20 keV, provides evidence of such coupling. Also, the plasma distributions in Fig. 8(a) are considerably smeared out compared to the beam-injected distribution in Fig. 8(c), which is again evidence of diffusion. Electron drag, however, lowers particle energies causing filling in of the distribution below injection energy so the evidence for diffusion is not as compelling as the 25 keV argument. The beam distribution in Fig. 8(c) has been computed from the beam extraction voltages, assuming a mixture of 0.5 full energy, 0.4 half energy and 0.1-third energy atomic D^0 components. These fractions have been measured

by the LBL neutral beam group.[5] The strongest evidence of quasi-linear saturation comes with observed increase of ion diffusion with wave amplitude when the plasma stream is shut off. Since the neutral beam trapping rate matches the plasma loss rate before the stream is turned off, according to the theory, the density decay rate after the stream is turned off is to be explained by an increase in ion-energy diffusion. This is seen in the behavior of the 40 keV charge-exchange signal in Fig. 2(d) and again in Fig. 10 where we have shown charge-exchange flux signals at E = 1.4, 2.6, 5.9, 17.6, 25, and 39 keV. For the data shown in Fig. 10, the line density buildup was similar to that in Fig. 2(a), reaching $4.3 \times 10^{14}/cm^2$ before the stream was shut off, and then decaying with a 0.38 ms decay time. The injected beam current was 250 amps. The increase in diffusion after the stream is shut off is particularly evident in the 25 and 39 keV channels in Fig. 10 which initially show a large increase in magnitude. The subsequent decrease 0.3 to 0.4 ms after the stream is turned off causes the distribution to decay in all channels. The increase observed in the 39 keV signal is delayed approximately 0.1 ms relative to the 25 keV signal. This is evidence of ion diffusion upward in energy from the bulk of the ion distribution. At 17 keV and below, termination of the plasma stream causes an immediate decrease in signal as diffusion out of these channels exceeds diffusion and beam injection into them.

To estimate the diffusion coefficient in Eq. (4) this data has been simulated with the quasi-linear computer codes that have been developed to model the 2XIIB experiment. A description of the 1-D code by Berk and Stewart describing evolution of the perpendicular ion energy distribution is given in Ref. 17. A similar 2-D code treating also the velocity component parallel to the magnetic field has been developed by T. Roglien (report in preparation). For the comparison to be presented we have used the 2-D code which treats the velocity components parallel and perpendicular to the magnetic

field. The 1-D code gives similar results. Since the sensitivities of the 25 and 39 keV channels were not calibrated at the time the data in Fig. 10 were obtained, we have compared the theoretical and experimental decay rates $\frac{1}{F(E,t)} \frac{\partial F(E,t)}{\partial t}$ in Fig. 11 at various energies. The theory is seen to match the data reasonably well at the 25 and 39 keV energy channels where both show increasing signals, and at intermediate energies where the decay rate is relatively independent of energy and corresponds closely to the experimental density decay rate. At low energies the experimental data appear to decay more rapidly than the theoretical model. For the comparison shown in Fig. 11, the values of $D(E_\perp)$ before and after the stream is turned off are given respectively by:

$$D(E_\perp) = \frac{2.1 \times 10^6}{E_\perp^{\frac{1}{2}}} \text{ keV}^2/\text{s} \quad \text{and} \quad D(E_\perp) = \frac{5.5 \times 10^6}{E_\perp^{\frac{1}{2}}} \text{ keV}^2/\text{s}$$

for $E_\perp > 4$ keV and for $E_\perp$ measured in keV. Below 4 keV the asympototic expansion of the Bessel function appearing in D (Eq. (5)), is not valid and $D(E_\perp)$ approaches a linear dependence on $E_\perp$ (the sum over Bessel functions contains only the first harmonic).

For comparison with the plasma time scales in Table 1 we define a diffusion time $\tau_D = \frac{E_\perp^2}{D(E_\perp)}$. This is plotted in Fig. 12 where we have also indicated the transit time $\frac{\sqrt{\pi} L_p}{\sqrt{\left(\frac{2E}{M_i}\right)}}$ of a particle for a plasma length $\sqrt{\pi} L_p = 25$ cm. For $E_\perp \leq 1$ keV, the diffusion time is less than the transit time of a particle through the plasma. It is this property that allows the plasma to reach a marginally stable state by filling the ambipolar hole .

V. Conclusions

We have measured the frequency and wavelength of electrostatic ion cyclotron oscillations in a stream stabilized neutral beam injected mirror machine. A narrow band $\frac{\Delta f}{f} < 0.02$ single-mode spectrum near the ion cyclotron frequency is observed. For most of the time evolution of plasma density buildup and decay, the wave propagates in the direction of the ion-diamagnetic drift with $2.9 < k_\perp a_i < 6.1$. Ion energy diffusion is present while the plasma is stream-stabilized and is observed to increase markedly when the plasma is de-stabilized by turning off the axially injected plasma stream. The increase in diffusion occurs simultaneously with a buildup in the amplitude of ion cyclotron oscillations and increase in plasma loss rate with no change in the spectral wave properties. These observations are in accord with a wave particle model of saturation of the drift cyclotron loss cone (DCLC) mode. The measured frequency of oscillation is less than the vacuum field ion cyclotron frequency. The shift from the cyclotron frequency corresponds closely to the finite beta field depression calculated for the center plasma density. The plasma density decay when the stabilizing stream is shut off is observed to begin at the plasma center and move radially outward. Very early and late in time, the ion cyclotron wave propagates opposite the ion-diamagnetic direction and this has not been explained by the DCLC dispersion relation.

ACKNOWLEDGEMENT

The author is indebted to T. D. Rognlien for many helpful discussions and critical comments on the manuscript, and for permission to use the quasi-linear computer code results plotted in Fig. 10. He also acknowledges the collaboration of E. J. Powers and T. C. Simonen on the wave measurements presented in Section IV, and is grateful to T. C. Simonen for helpful comments on the manuscript.

References

1. F. H. Coensgen, W. F. Cummins, B. G. Logan, A. W. Molvik, W. E. Nexsen, T. C. Simonen, B. W. Stallard, W. C. Turner, Phys. Rev. Lett., 35, 1501. (1975)

2. M. S. Ioffe, B. I. Kanaev, V. P. Pastukhov, E. E. Yushmanov, Sov. Phys. JETP, 40, 1064. (1975)

3. D. E. Baldwin, H. L. Berk, L. D. Pearlstein, Phys. Rev. Lett., 36 1051. (1976)

4. R. F. Post, M. N. Rosenbluth, Phys. Fluids, 9, 730. (1966)

5. W. R. Baker, K. H. Berkner, W. S. Cooper, K. W. Ehlers, W. B. Kunkel, R. V. Pyle, J. W. Stearns, Proc. of Fifth Conf. on Plasma Physics and Cont. Nucl. Fusion Research, Tokyo, 1974 (IAEA, Vienna, 1975)

6. F. H. Coensgen, W. F. Cummins, C. Gormezano, B. G. Logan, A. W. Molvik, W. E. Nexsen, T. C. Simonen, B. W. Stallard, W. C. Turner, Phys. Rev. Lett., 37, 143 (1976)

7. B. G. Logan, J. F. Clauser, F. H. Coensgen, D. L. Correll, W. F. Cummins, C. Gormezano, B. G. Logan, A. W. Molvik, W. E. Nexsen, T. C. Simonen, W. C. Turner, Phys. Rev. Lett., 37, 1468.(1976)

8. W. E. Nexsen, B. G. Logan, F. H. Coensgen, A. W. Molvik, W. F. Cummins, Bull. Am. Phys. Soc.,20, 1232. (1975)

9. W. M. Tang, L. D. Pearlstein, H. L. Berk, Phys. Fluids, 15, 1153. (1972)

10. A. W. Molvik, Bull. Am. Phys. Soc.,21, 1147. (1976)

11. F. H. Coensgen, J. F. Clauser, D. L. Correll, W. F. Cummins, C. Gormezano, B. G. Logan, A. W. Molvik, W. E. Nexsen, T. C. Simonen, B. W. Stallard, W. C. Turner, Proc. Sixth Conf. on Plasma Physics and Cont. Nucl Fusion Research, Berchtesgaden, 1976 (IAEA, Vienna, 1977)

12. J. F. Clauser, C. Gormezano, W. E. Nexsen, T. C. Simonen, W. C. Turner, Bull. Am. Phys, 21, 1143. (1976)

13. L. Spitzer, Physics of Fully Ionized Gases, 2nd. ed., Interscience 1962

14. D. E. Baldwin, C. O. Beasley, H. L. Berk, W. M. Farr, R. C. Harding, J. E. McCune, L. D. Pearlstein, A. Sen, Proc. Fourth Conf. on Plasma Physics and Cont. Nucl. Fusion Research, Madison, 1971 (IAEA, Vienna, 1972)

15. A. A. Galeev, Proc. of Third Conf. on Plasma Physics and Cont. Nucl. Fusion Research, Culham, 1965 (IAEA, Vienna, 1966)

References(continued)

16. F. H. Coensgen, W. F. Cummins, A. W. Molvik, W. E. Nexsen, T. C. Simonen, B. W. Stallard, Proc. of Fifth Conf. on Plasma Physics and Cont. Nucl. Fusion Research, Tokyo, 1974 (IAEA, Vienna, 1975)

17. H. L. Berk, J. J. Stewart, to be published in July 1977 Phys. Fluids.

18. T. C. Simonen, R. H. Bulmer, F. H. Coensgen, W. F. Cummins, C. Gormezano, B. G. Logan, A. W. Molvik, W. E. Nexsen, B. W. Stallard, W. C. Turner, G. E. Vogtlin, R. R. Vandervoort, Journal of Nucl. Materials, 63, 59. (1976)

19. T. C. Simonen, Phys. Fluids, 19, 1365 (1976)

20. D. Smith, E. J. Powers, IEEE Trans., Plasma Sci., 2, 261. (1974)

21. J. C. Sprott, Rev. Sci. Inst., 37, 897. (1966)

22. E. J. Powers, T. C. Simonen, J. Appl. Phys., 47, 3911. (1976)

23. E. O. Brigham, The Fast Fourier Transform, Prentice-Hall, Inc., 1974.

24. H. Hendel, M. Yamada, Phys. Rev. Lett., 33, 10.E. (1974)

25. M. N. Rosenbluth, Phys. Rev. Lett., 29, 408. (1972)

26. R. Aamodt, Phys. Rev. Lett., 27, 135. (1971)

FIGURE CAPTIONS

Fig. 1 Schematic of 2XIIB illustrating:
- (a) injection of plasma stream and
- (b) injection of gas at a mirror throat

Fig. 2 Plasma Measurements vs. Time with Stream Stabilization
- (a) line density
- (b) mean ion energy
- (c) 40 keV charge exchange signal
- (d) amplitude of rf oscillations

Fig. 3 Schematic of rf probe system

Fig. 4 (a) Cross power amplitude spectrum $P_{21}(f)$

(b) Cross power phase spectra $\theta_{21}(f)$, $\theta_{31}(f)$, $\theta_{41}(f)$, $\theta_{51}(f)$.

At f = 4.50 MHz, θ_{21} = .38, θ_{31} = .84, θ_{41} = 1.71, θ_{51} = 2.49 radians.

Fig. 5. Wave Numbers vs. Time of Measurement

Dashed line is the condition

$$k_i^* = k_\perp \frac{cE_i}{eB_{vac}} \frac{1}{R_p} \text{ equals } \omega_{ci} = \frac{eB_{vac}}{M_i c}$$

for $\bar{E}_i$ = 13 keV, B_{vac} = 6.4 kg, R_p = 7. cm

Fig. 6. The frequency shift $\Delta f = f - f_{ci\ vac}$ of measured frequency from the vacuum ion cyclotron frequency vs. the product of mean ion energy and plasma line density $\bar{E}_i \cdot \int n dt$. The horizontal axis at the top of the figure indicates the center plasma beta $\beta(0) = 8\pi \frac{n(0)\bar{E}_i}{B_{vac}^2}$

Fig. 7. Line density profiles measured by beam attenuation in the vertical plasma midplane. Smooth curve is a Gaussian profile e^{-x^2/R_p^2} for a mean plasma radius

$$R_p = \frac{1}{n(0)} \int n(x, y = 0, z = 0)\, dx$$ equal to 7 cm.

FIGURE CAPTIONS
(continued)

Fig. 8. (a) Measured ion energy distribution at t = 2.8 ms and t = 4.0 ms in Fig. 2. The cross-hatched area is the region where ion speed equals $\frac{\omega}{k_\perp}$ measured in Fig. 5.

(b) Plot of ion energy distribution $F(E_\perp) = H(E_\perp - e\phi)E_\perp e^{-E_\perp/E_H}$ used in analysis of DCLC dispersion relation. $e\phi$ = 0.50 keV, E_H = 6.0 keV.

(c) Plot of energy distribution of neutral beam atoms.

Fig. 9. Solution to the DCLC dispersion relation for Re $\omega = \omega_{ci}$(a) $k_\perp$ vs. E_w, (b) $k_\perp$ vs. $e\phi$ (c) $k_\perp$ vs. $\langle E_\perp \rangle$.

Fig. 10 Charge exchange analyzer signals vs. time. Stream plasma is shut off at t = 3.8 ms.

Fig. 11 Energy dependent decay rate $\frac{1}{F(E_\perp,t)} \frac{\partial F(E_\perp,t)}{\partial t}$ after stream shuts off. Closed circles are experimental data, open circles are from 2-D quasi-linear computer model. The dashed line is the experimentally observed density decay rate $\frac{1}{n}\frac{dn}{dt} = -2.6 \times 10^3$ sec^{-1}.

Fig. 12 The diffusion time $\tau_D = \frac{E_\perp^2}{D(E_\perp)}$ vs. ion energy. Dashed lines indicate the transport times in Table 1.

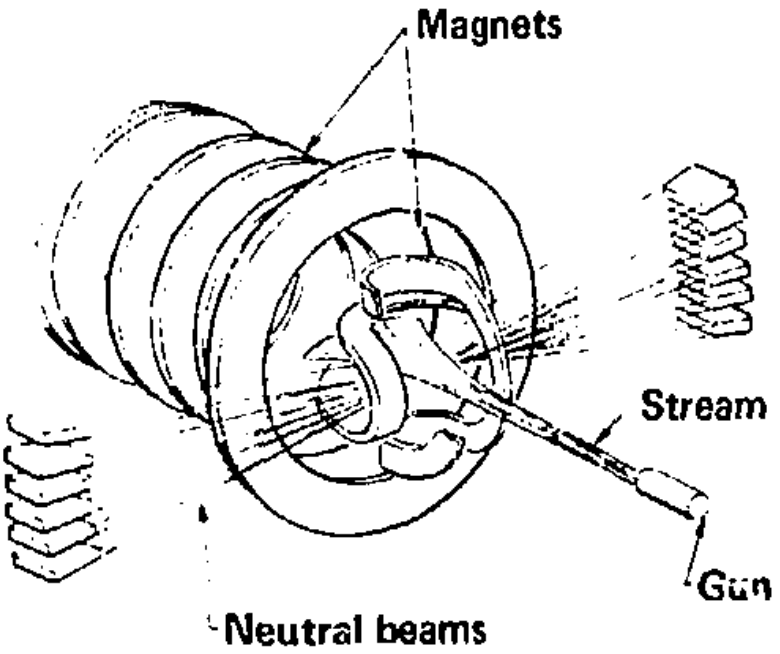
Magnets
Stream
Gun
Neutral beams
(a)

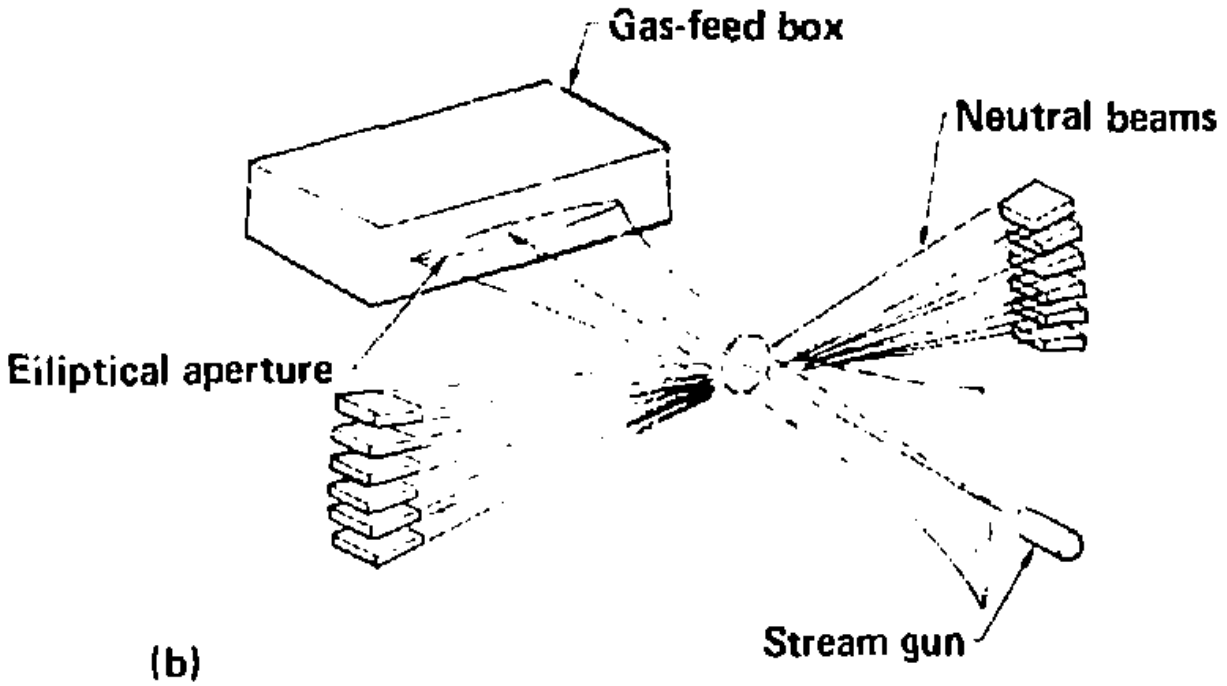
Gas-feed box
Neutral beams
Eiliptical aperture
Stream gun
(b)

Figure 1.

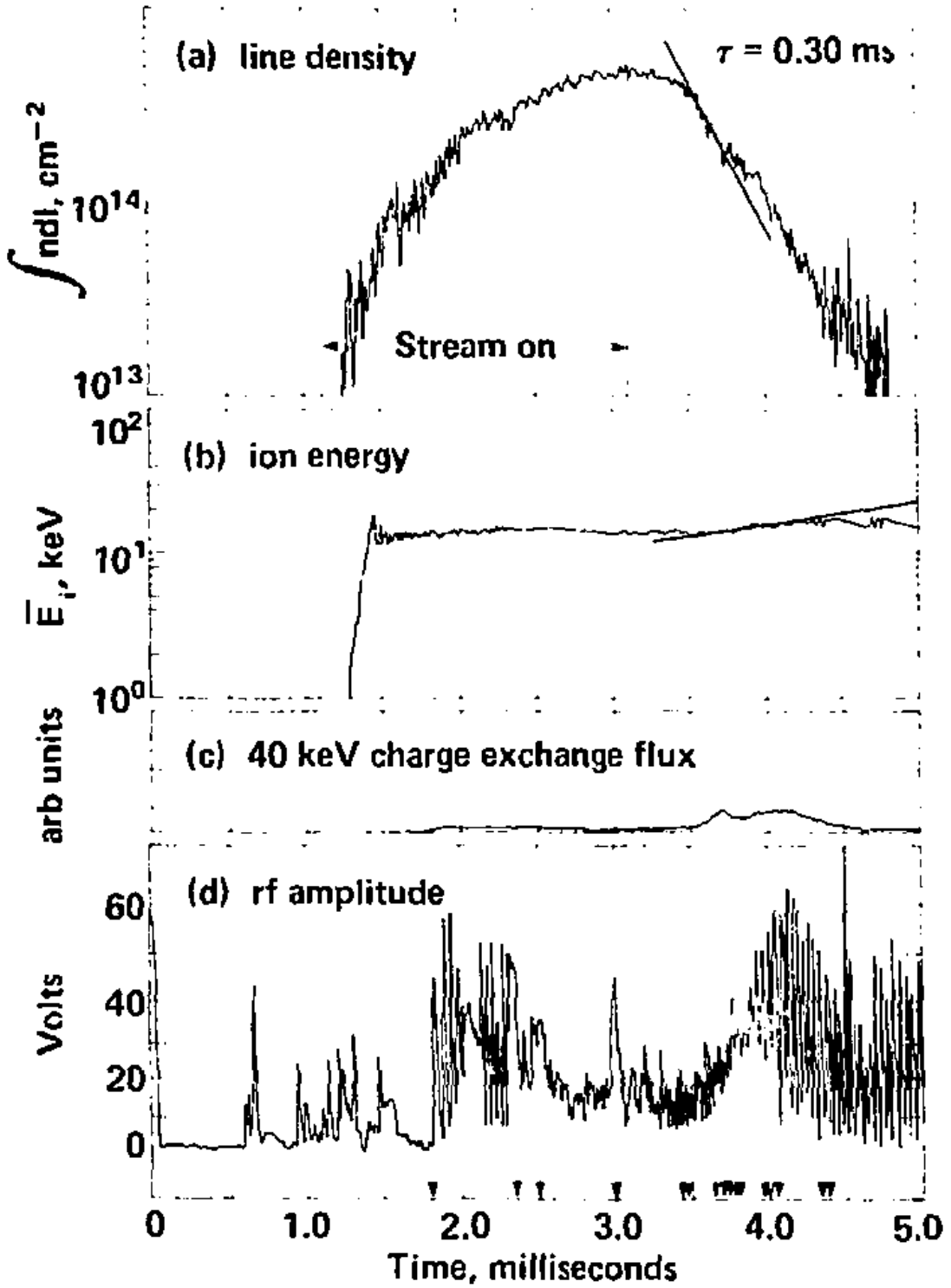
(a) line density
τ = 0.30 ms
$\int ndl$, cm^{-2}
10^{14}
10^{13}
Stream on
(b) ion energy
10^2
10^1
10^0
$\bar{E}_i$, keV
(c) 40 keV charge exchange flux
arb units
(d) rf amplitude
60
40
20
0
Volts
0
1.0
2.0
3.0
4.0
5.0
Time, milliseconds

Figure 2.

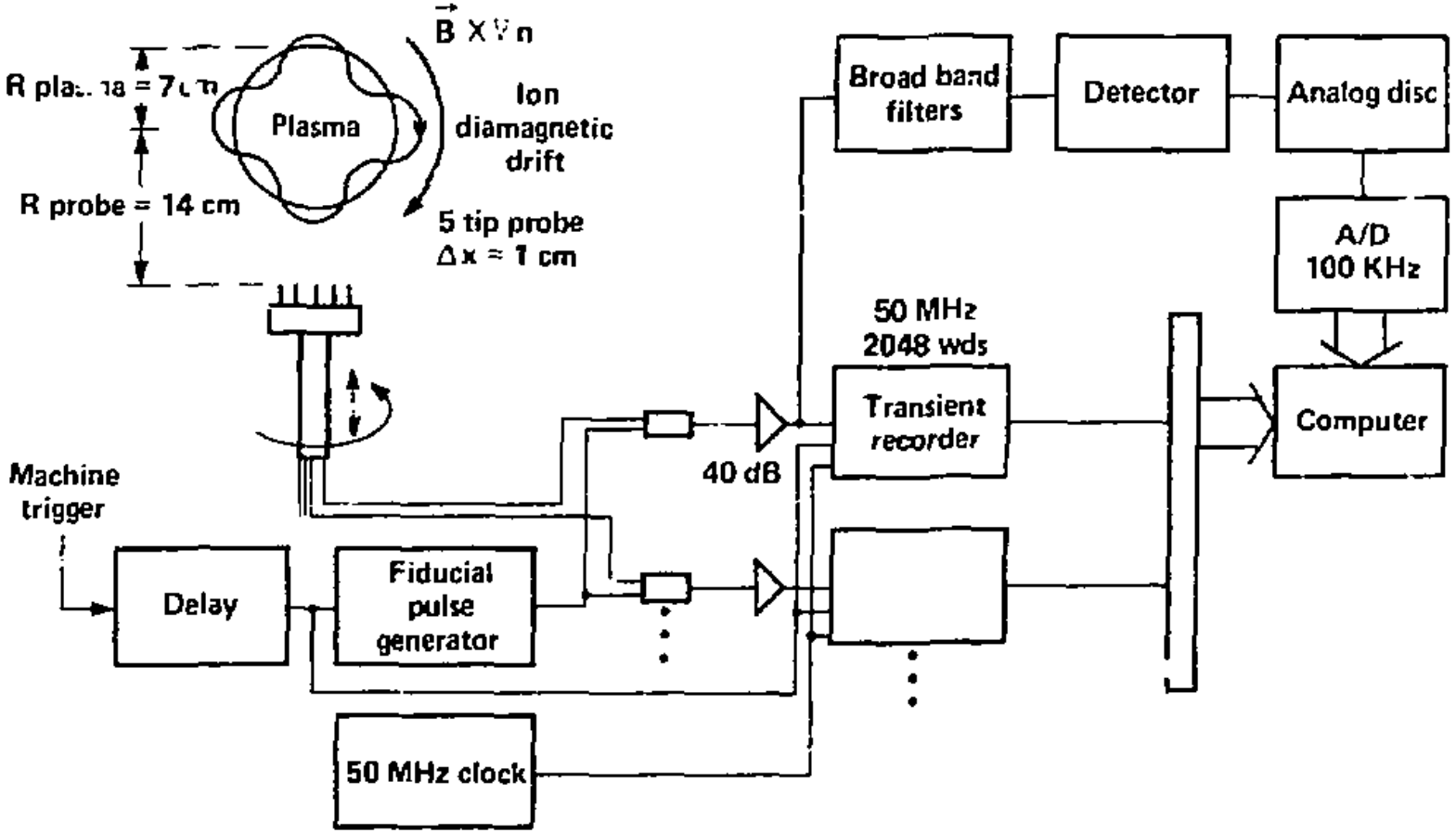
$\vec{B} \times \nabla n$
R plasma = 7 cm
Plasma
Ion diamagnetic drift
R probe = 14 cm
5 tip probe
Δx = 1 cm
Broad band filters
Detector
Analog disc
A/D 100 KHz
50 MHz 2048 wds
Transient recorder
Computer
40 dB
Machine trigger
Delay
Fiducial pulse generator
50 MHz clock

Figure 3.

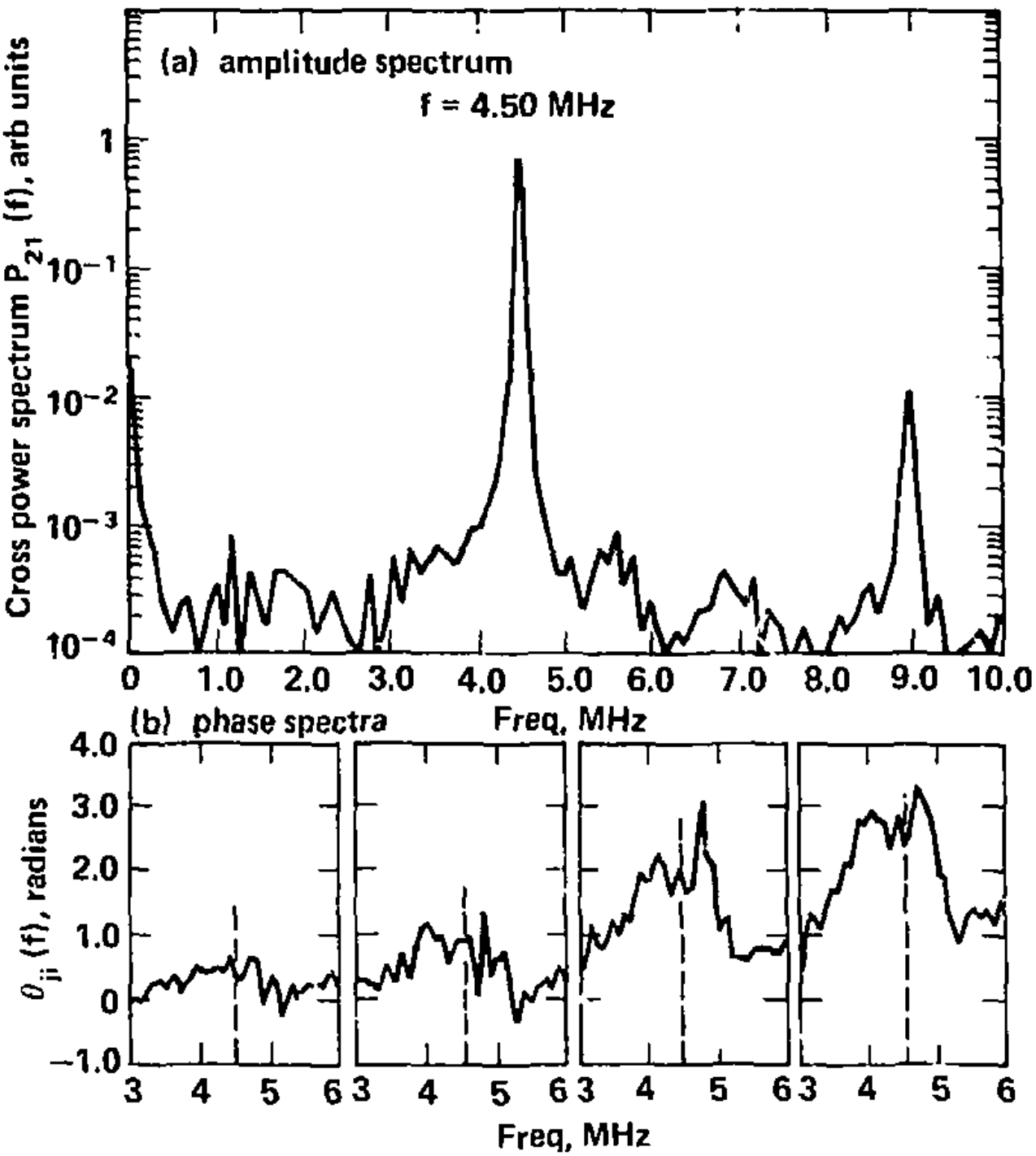
(a) amplitude spectrum
f = 4.50 MHz
Cross power spectrum P_{21} (f), arb units
1
10^{-1}
10^{-2}
10^{-3}
10^{-4}
0 1.0 2.0 3.0 4.0 5.0 6.0 7.0 8.0 9.0 10.0
Freq, MHz
(b) phase spectra
θ_{ji} (f), radians
4.0
3.0
2.0
1.0
0
−1.0
3 4 5 6 3 4 5 6 3 4 5 6 3 4 5 6
Freq, MHz

Figure 6.

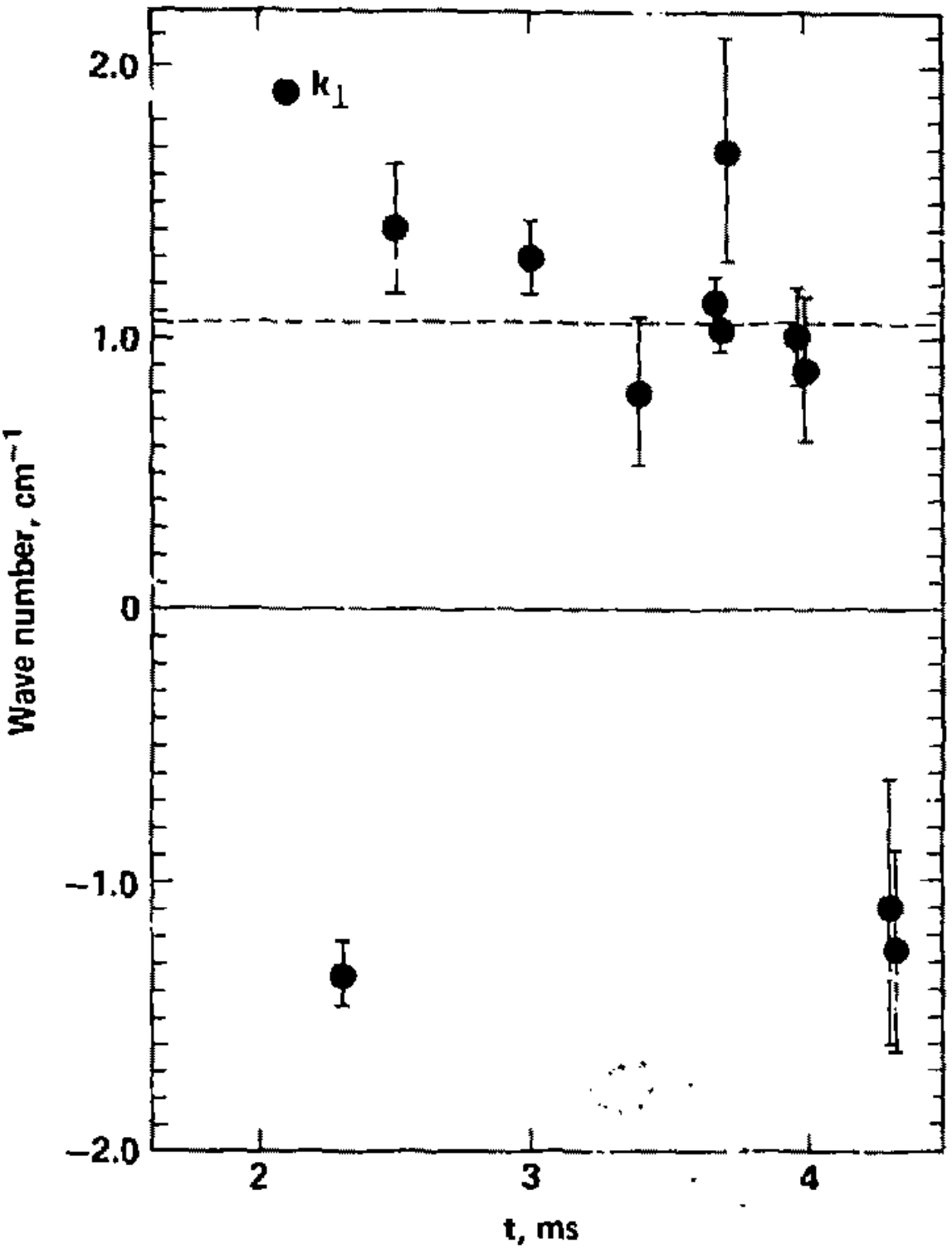

Figure 5.

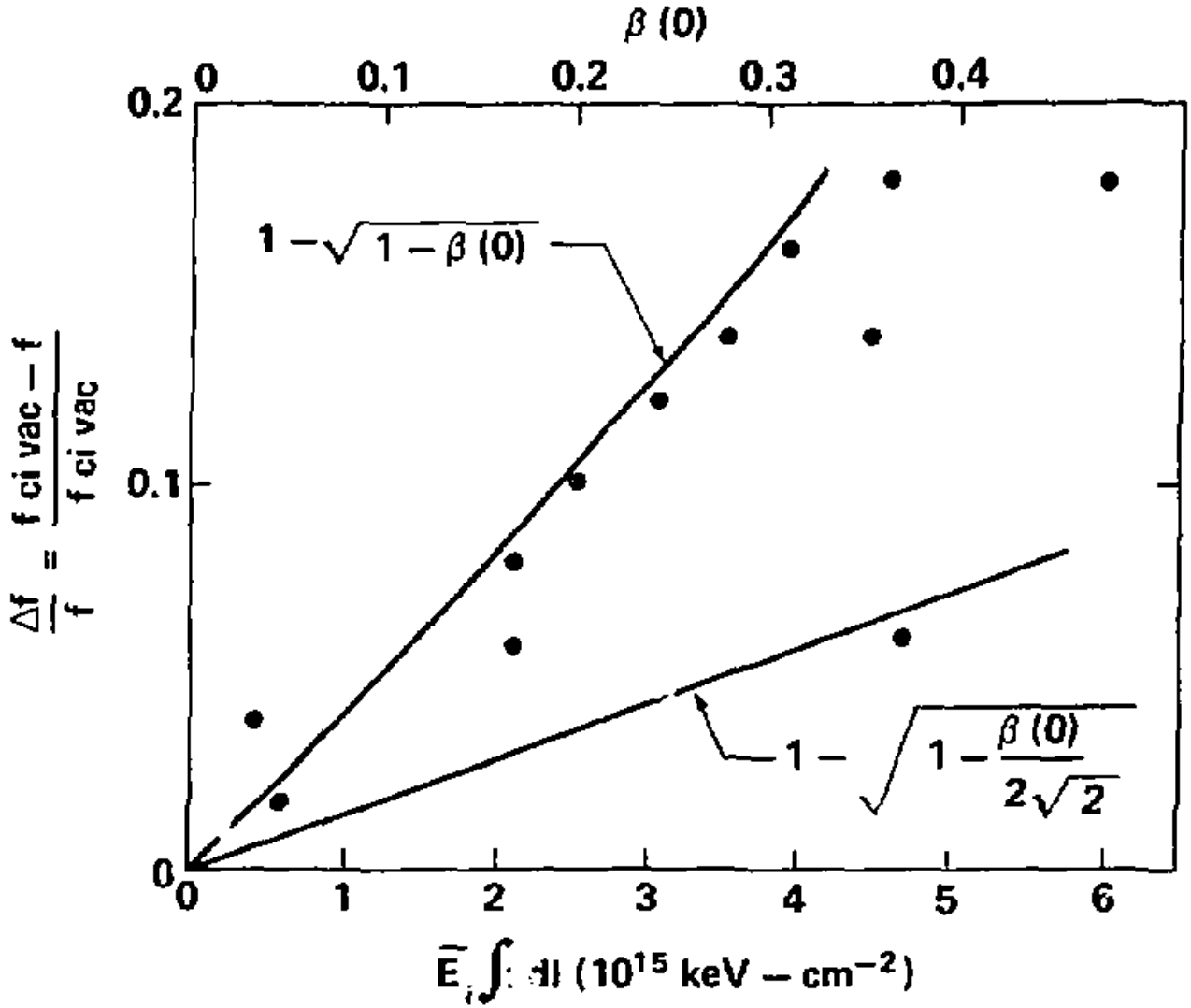
β (0)
0
0.1
0.2
0.3
0.4
0.2
0.1
0
$\frac{\Delta f}{f} = \frac{f_{ci\ vac} - f}{f_{ci\ vac}}$
$1 - \sqrt{1 - \beta(0)}$
$1 - \sqrt{1 - \frac{\beta(0)}{2\sqrt{2}}}$
0
1
2
3
4
5
6
$\bar{E}_i \int dl\ (10^{15}\ keV - cm^{-2})$

Figure 6.

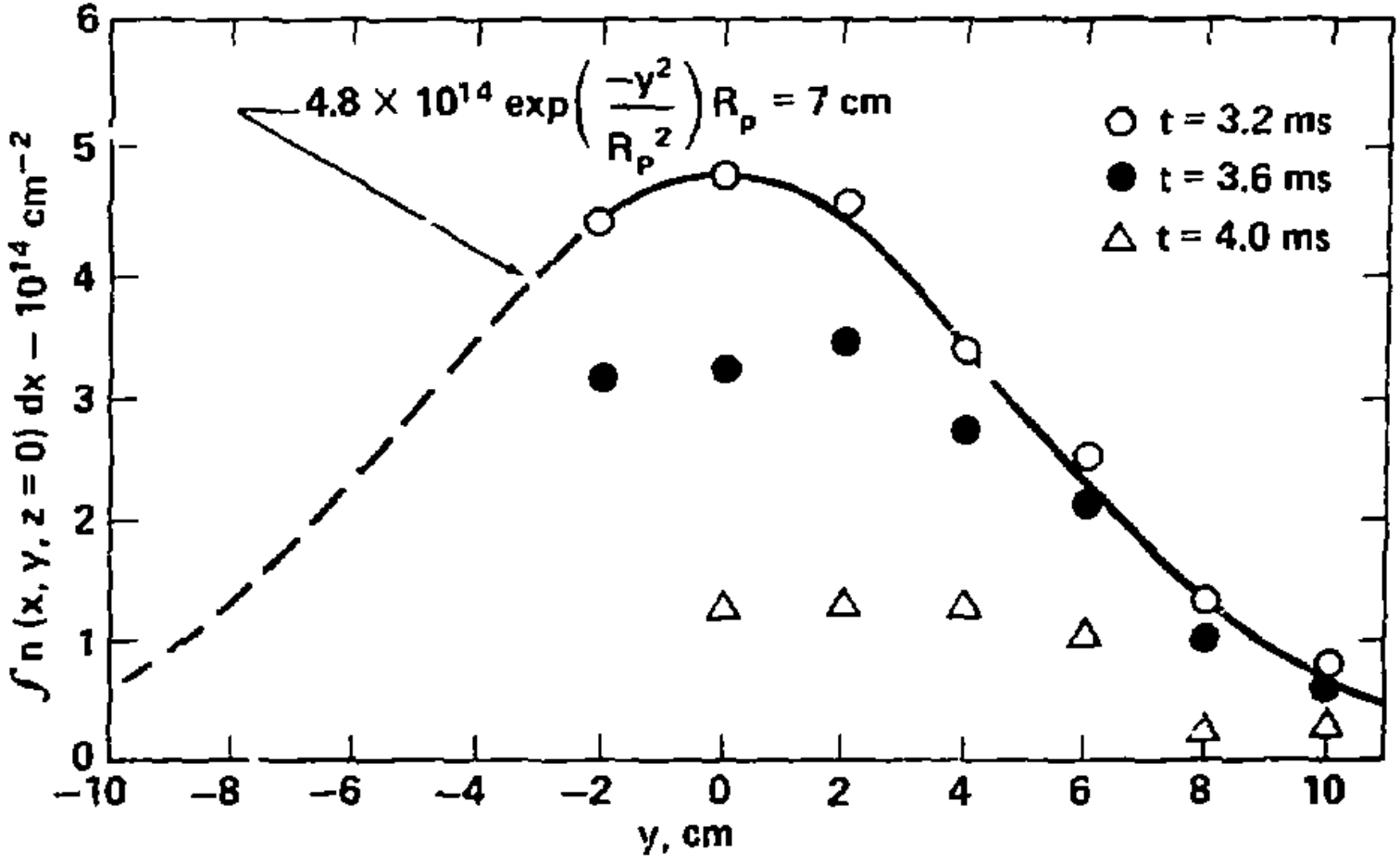
$4.8 \times 10^{14} \exp\left(\frac{-y^2}{R_p^2}\right) R_p = 7$ cm
t = 3.2 ms
t = 3.6 ms
t = 4.0 ms
$\int n(x, y, z=0)\, dx - 10^{14}\ cm^{-2}$
y, cm
6
5
4
3
2
1
0
−10
−8
−6
−4
−2
0
2
4
6
8
10

Figure 7.

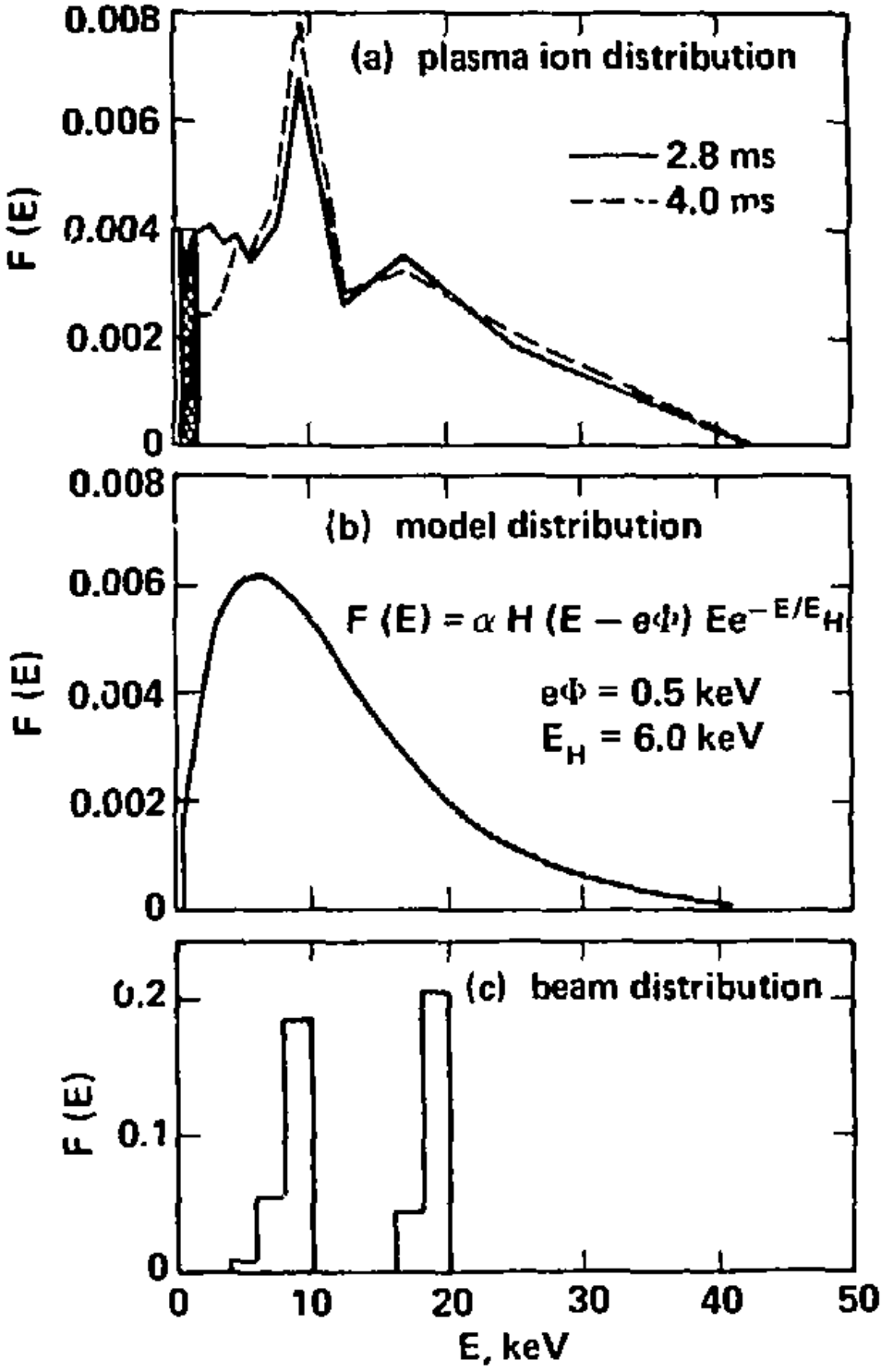
(a) plasma ion distribution
2.8 ms
4.0 ms
F (E)
0.008
0.006
0.004
0.002
0
(b) model distribution
F (E) = α H (E − eΦ) Ee^−E/E_H
eΦ = 0.5 keV
E_H = 6.0 keV
(c) beam distribution
0.2
0.1
0
10
20
30
40
50
E, keV

Figure 8.

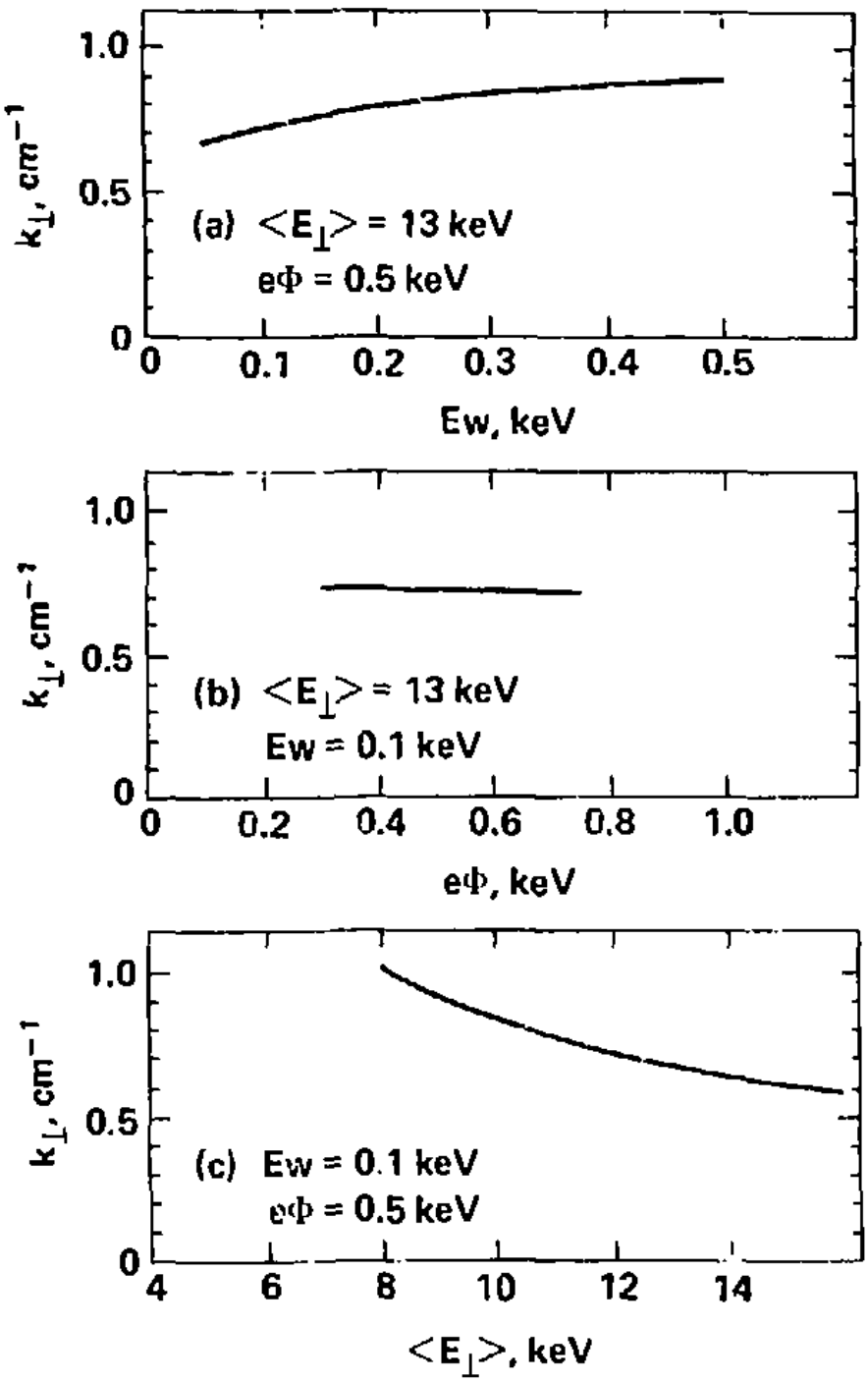
1.0
0.5
0
$k_\perp$, cm^{-1}
(a) $\langle E_\perp \rangle$ = 13 keV
eΦ = 0.5 keV
0
0.1
0.2
0.3
0.4
0.5
Ew, keV
1.0
0.5
0
$k_\perp$, cm^{-1}
(b) $\langle E_\perp \rangle$ = 13 keV
Ew = 0.1 keV
0
0.2
0.4
0.6
0.8
1.0
eΦ, keV
1.0
0.5
0
$k_\perp$, cm^{-1}
(c) Ew = 0.1 keV
eΦ = 0.5 keV
4
6
8
10
12
14
$\langle E_\perp \rangle$, keV

Figure 9.

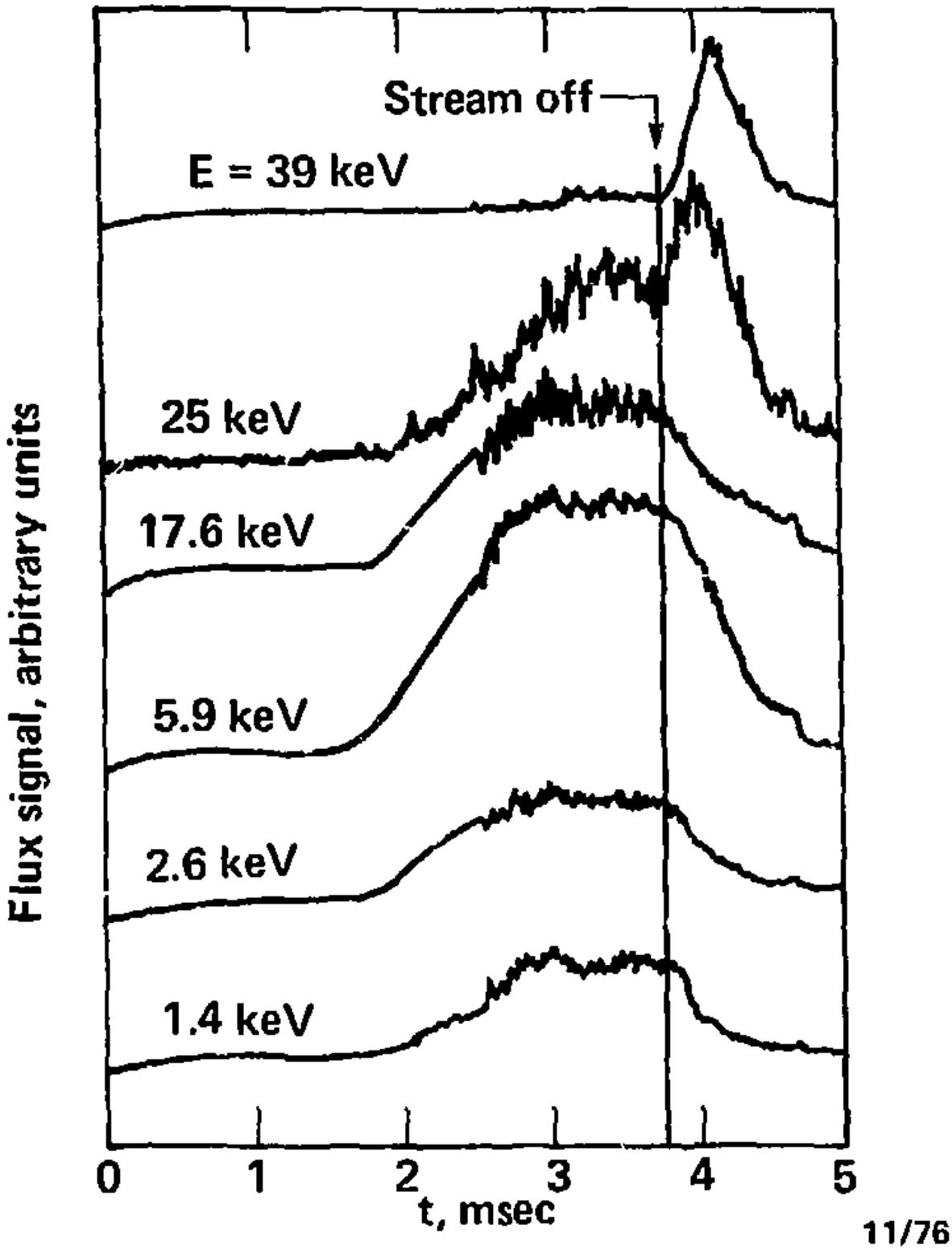
Stream off
E = 39 keV
25 keV
17.6 keV
5.9 keV
2.6 keV
1.4 keV
Flux signal, arbitrary units
0
1
2
3
4
5
t, msec
11/76

Figure 10.

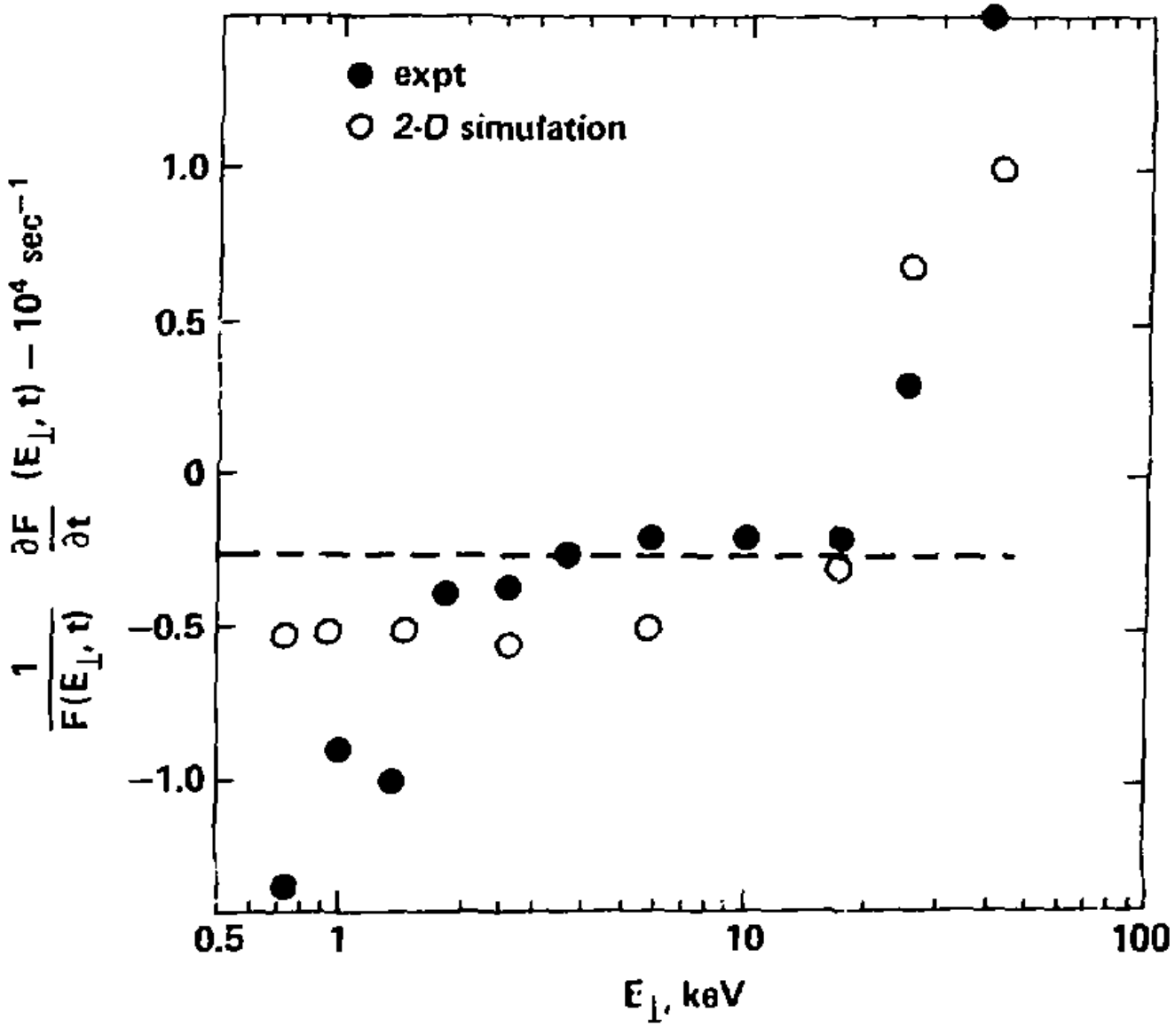
expt
2-D simulation
1.0
0.5
0
−0.5
−1.0
0.5
1
10
100
$E_\perp$, keV
$\frac{1}{F(E_\perp, t)} \frac{\partial F}{\partial t} (E_\perp, t) - 10^4 \text{ sec}^{-1}$

Figure 11.

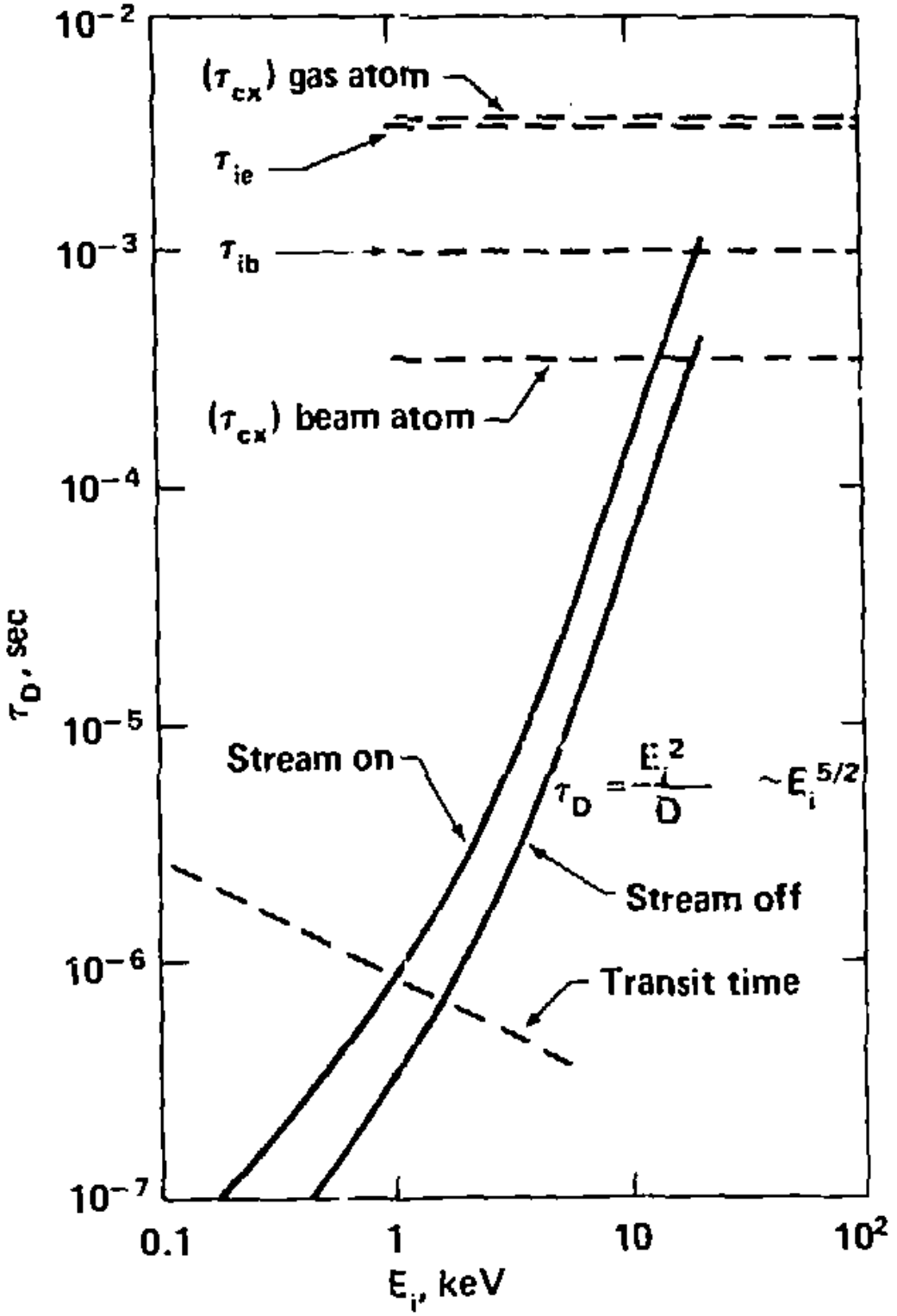
10^{-2}
(τ_{cx}) gas atom
τ_{ie}
10^{-3}
τ_{ib}
(τ_{cx}) beam atom
10^{-4}
τ_D, sec
10^{-5}
Stream on
$\tau_D = \frac{E_i^2}{D}$
$\sim E_i^{5/2}$
Stream off
10^{-6}
Transit time
10^{-7}
0.1
1
10
10^2
E_i, keV

Figure 12.